Korean J. Chem. Eng., 39(4), 1053-1064 (2022)
DOI: 10.1007/s11814-021-0940-z

pISSN: 0256-1115
eISSN: 1975-7220

Composites derived from synthetic clay and carbon sphere: Preparation, characterization, and application for dye decontamination

Nguyen Duy Dat*, Ton That Loc,***, Mai Thuan Trieu*, Dong Thanh Nguyen****, Khuong Quoc Nguyen*****, My Linh Nguyen*, Anh Duy Duong Le******,*******, and Hai Nguyen Tran**,***,†**

*Faculty of Chemical & Food Technology, Ho Chi Minh City University of Technology and Education, Thu Duc, Ho Chi Minh, 700000, Vietnam
**Institute of Fundamental and Applied Sciences, Duy Tan University, Ho Chi Minh, 700000, Vietnam
***Faculty of Environmental and Chemical Engineering, Duy Tan University, Da Nang, 550000, Vietnam
****Institute of Environmental Technology, Vietnam Academy of Science and Technology, Hanoi, Vietnam
*****Department of Crop Science, College of Agriculture, Can Tho University, Can Tho, Vietnam
******Computational Optics Research Group, Advanced Institute of Materials Science, Ton Duc Thang University, Ho Chi Minh City, Vietnam
*******Faculty of Applied Sciences, Ton Duc Thang University, Ho Chi Minh City, Vietnam
(*Received 4 July 2021 • Revised 20 August 2021 • Accepted 24 August 2021*)

Abstract−Two new composites from synthetic clay-like materials and carbon spheres were developed. Layered doubled hydroxides (LDH) were synthesized from the coprecipitation of Mg^{2+} and Al^{3+} ions. Spherical hydrochar (SH) was prepared from pure glucose through hydrothermal carbonization at 190 °C. The composite LDH–SH was synthesized through a simple hydrothermal method of the mixture of LDH and SH. Another composite, LDO-SB, was directly prepared through the carbonization of LDH-SH at 500 °C. Under such high temperature, LDH was converted to layered doubled oxides (LDO), and SH was transferred to spherical biochar (SB). Those materials were characterized by chemical stability, surface morphology and element composition, crystal structure, surface functional group, and textural characteristic. They were applied for removing cationic dye (methylene blue; MB) and anionic dye (Congo red; CR) under different pH solutions. Three adsorption components—kinetics, isotherm, and thermodynamics—were conducted under batch experimenters. Results demonstrated that the LDH or LDO particles were assembled on the surface of SH or SB, respectively. The surface area, total pore volume, and average pore width of LDH–SH and LDO-SB were 58.5 and 198 m^2/g, 0.319 and 0.440 cm^3/g, and 21.8 and 8.89 nm, respectively. The maximum adsorption capacity of the materials, calculated from the Langmuir model, at 30 °C for CR and MB dyes was 1589 and 78.6 mg/g (LDO-SB) and 499 and 226 mg/g (LDH-SH), respectively. The composites exhibited a higher affinity to anionic than cationic dyes, which resulted from the great contribution of the clay-like materials. Therefore, they can serve as a promising composite for the decolorization of wastewater.

Keywords: Adsorption, Composite, Layered Doubled Hydroxide, Layered Doubled Oxide, Carbon Sphere

INTRODUCTION

Nanomaterials have attracted much attention from the scientific community because of their wide applications. Although they have been investigated and applied for water purification, there are still some existing problems, such as separation and human health concerns [1,2].

Among current nanomaterials, layered double hydroxides (LDH) with their nanostructured nature, also known as synthesized clays, have been acknowledged as an excellent nanomaterial for water treatment [3]. Galvão et al. [4] reported the hydrodynamic particle size determined by the dynamic light scattering particle size of Zn/Al-LDH under different conditions of co-precipitation ranging from 331 nm to 913 nm. Some previous studies showed that nanostructured LDH-based adsorbents exhibited a high affinity to adsorbate anions (organic and inorganic) in water such as Congo red dye [5-8], methyl orange dye [8,9], reactive red dye [10], acid red 1, [10], acid red G [11], Cr(VI) ions [6], and phosphate [12]. This is because of their unique chemical structure. In general, LDH is commonly synthesized by the coprecipitation method of two salts: M^{2+} and M^{3+} [4,10,13]. The general formula of LDH materials can be expressed as $[M_{1-x}^{2+}M_x^{3+}(OH)_2]^{x+}(A^{n-})_{x/n}{\cdot}mH_2O$. In this chemical composition, M^{2+} and M^{3+} indicate divalent (i.e., Zn^{2+}, Ca^{2+}, Mg^{2+}, and Mg^{2+}) and trivalent (i.e., Cr^{3+}, Al^{3+}, and Fe^{3+}) metal cations; meanwhile, x is the molar ratio of two salts of $M^{3+}/(M^{2+}+M^{3+})$. The A^{n-} symbol is the anions (A) in their interlayer region with a relevant charge of valence n (i.e., CO_3^{2-} and NO_3^-) [2,4,11,14,15].

Notably, under high calcinated temperatures (i.e., 500 °C), layered double hydroxides (LDH) were converted to layered double

†To whom correspondence should be addressed.
E-mail: trannguyenhai@duytan.edu.vn, trannguyenhai2512@gmail.com

oxides (LDO). LDO can be recrystallized to LDH when using suitable regenerated solutions or even deionized water [9,16]. This rehydration is obtained due to its unique characteristics (commonly known as "memory effect" or "structural memory") [6,9,14,16,17]. In addition, the crystal size of LDO, determined by the X-ray powder diffraction technique, is often smaller than that of LDH. For example, Gao et al. [16] reported that the crystallite size of Mg/Al-LDO and Zn/Al-LDO, determined by the X-ray powder diffraction technique, was 13.7 and 28.0 nm; meanwhile, that of Mg/Al-LDH and Zn/Al-LDH was 46.8 nm and 19.9 nm, respectively. Therefore, it will take more time to sedimentate or separate them from water after decontamination.

To solve the problem of separation and enhance removal efficiency, some authors have tried to develop composites derived from LDH or LDO. For example, Kazeem et al. [9] developed two composites, one from graphene and LDH and another from graphene and LDO, and applied them for decolorizing methyl orange dye from water. Yang et al. [12] reported that the composites synthesized from corn stalk-generated biochar and LDH (i.e., Zn/Al-LDH, Mg/Al-LDH, or Ni/Fe-LDH) can enhance their removal efficiency to phosphorus in water. More information on the composites of biochar and LDH (or LDO) and their application for water treatment have been recently reviewed by authors [15]. However, almost all biochar materials used to generate the composites were derived from lignocellulosic material wastes. Thus, they are commonly known as a non-spherical biochar.

The classification of spherical biochar and non-spherical biochar is mainly based on their different surface morphology that is detected by the scanning or transmission electron microscopy images [18]. Huang et al. [19] successfully prepared micro-nano carbon spheres from pure carbohydrate sources (xylose, glucose, and sucrose) through a common hydrothermal carbonization (HTC) method. The resultant solids after HTC are known as spherical hydrochar (SH). Spherical biochar [18] and spherical activated carbon [19,20] can be developed through a further treatment or activation of spherical hydrochar. Glucose-derived spherical biochar (SB) exhibited a larger surface area (1,292 m^2/g) and excellent adsorption capacity of paracetamol drug (286 mg/g) in water than pomelo peel-derived non-spherical biochar (1,033 m^2/g and 147 mg/g) [18]. In addition, carbon spheres exhibited a high content of oxygen-containing functional groups on their surface. Those groups can act as active sites to keep LDH or LDO on their surface. In fact, Huang et al. [19] reported that the isoelectric point (pH_{IEP} determined by the zeta potential curve) of carbon spheres was lower than 3.0. This means that they exhibit a negatively charged surface within pH solution higher than their pH_{IEP}. In contrast, LDH and LDO often have a high density of positively charged surface [4]. This is because their pH_{IEP} is often higher than 9.0 [2], such as pH_{IEP}>12 for Mg/Al-LDH [13].

Therefore, in this study, a composite, LDH-SH, was developed by the hydrothermal method of two different precursors: inorganic material (i.e., LDH) and organic material (SH). Another composite, LDO-SB, was directly obtained from LDH-SH through a further carbonization. They were characterized by various techniques and then applied for adsorbing different kinds of dyes, cationic and anionic, in water.

MATERIALS AND METHODS

1. Chemicals

Whole chemicals and reagents, which were used in this study, were of reagent grade. Therefore, they were utilized without any further purifying process. Congo red dye and methylene blue dye (Fig. S1) were purchased from Sigma-Aldrich. A pure carbohydrate source (glucose) that was bought from Merck was used for producing carbon spheres. Two metal salts, $AlCl_3$ and $MgCl_2{\cdot}6H_2O$, were obtained from Merck. They were used to synthesize clay-materials. The other common chemicals (i.e., NaOH, N_2CO_3, and HCl) were supplied from Scharlau.

2. Preparation of Composite Derived from Carbon Spheres and Clay-like Materials

Carbon spheres, SH and SB, were synthesized from the commercial pure carbohydrate (selected glucose) through a hydrothermal carbonization process (HTC) and subsequent pyrolysis (Fig. 1) [19]. Approximately 30 g of glucose was well dissolved in 100 mL distilled water. The mixture was transferred into a 150 mL-Teflon autoclave. The hydrothermal carbonization was conducted at 190 °C for 24 h. The brown solids obtained after HTC were washed repeatedly with distilled water and dried at 105 °C for 48 h. The dried particles (0.09-0.106 mm) were named as spherical hydrochar (SH). Meanwhile, spherical biochar (SB) was prepared from SH through the carbonization process at 500 °C for 3 h under an oxygen-limited condition. The resultant SH and SB were washed repeatedly with pure water until the pH of filtrate reached a constant value. More detailed information on the procedure for preparation of carbon spheres has been published by Tran et al. [18].

Clay-like materials (Mg/Al-LDH and Mg/Al-DO) were prepared

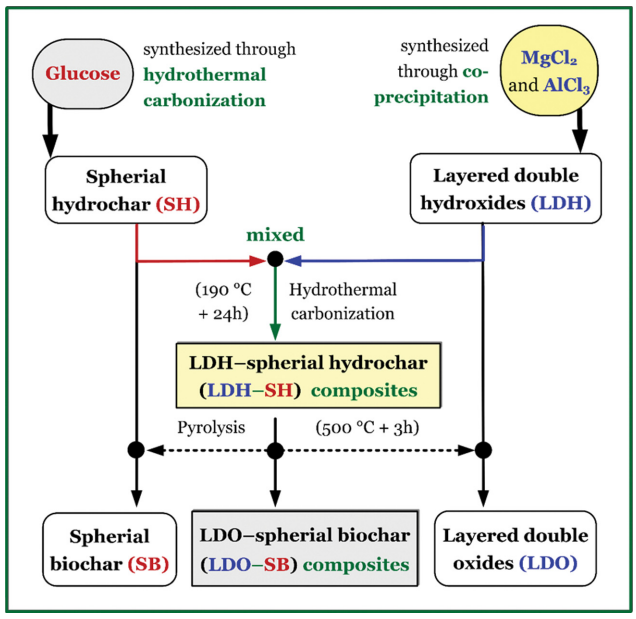

Fig. 1. Preparation process of the composites (LDH-SH and LDO-SB) and their feedstocks such as layered doubled hydroxides (LDH), layered doubled oxides (LDO), spherical hydrochar (SH), and spherical biochar (SB).

through a coprecipitation method of two salts ($MgCl_2$ and $AlCl_3$) and subsequent calcination (Fig. 1). The synthesis method has been reported elsewhere [13]. Briefly, the ratio of M^{2+} to M^{3+} was 3 : 1. The precipitation was conducted under a low supersaturation and a controlled pH 12 condition. The white nano-precipitates were collected, washed with distilled water, and then dried at 65 °C for 48 h. The dried particles were known as Mg/Al layered double hydroxides (Mg/Al-LDH). Meanwhile, calcinated layered double hydroxides (also known as layered double oxides; Mg/Al-LDO) were directly prepared from LDH through the calcination at 500 °C for 3 h.

Two composites (LDH-SH and LDO-SB) were prepared from clay-like materials and carbon spheres (Fig. 1). Around 4.0 g of SH was added to the water solution containing LDH (~4.0 g). The mixture was gently stirred at 30 °C for 4 h and then transferred into a Teflon autoclave. The autoclave was placed into a drying oven at 190 °C for 24 h. The mixture of LDH and SH (the LDH-SH composite) was then washed with distilled water and dried at 65 °C for 48 h. Notably, a primary test was done to evaluate the effect of the mass ratio of SH to LDH (0.5/1, 1/1, 1.5/1, and 2/1) on the adsorption capacity of the resultant LDH-SH composite to two CR and MB dyes. The initial result (data not shown) indicated that the LDH-SH composite prepared at the ratio of 1/1 exhibited the highest adsorption capacity to the dyes. Therefore, the optimal ratio for preparing LDH-SH was obtained at 1/1.

The LDO-SB composite was directly prepared from LDH-SH through the carbonization process under an oxygen-limited condition at 500 °C for 3 h. Under those conditions, LDH and SH were converted to LDO and SB, respectively. After calcination, the samples (LDO and LDO-SB) were cooled under oxygen-limited condition and stored in a desiccator for further uses. Importantly, the primary tests indicated that the washing process (using pure water) of the LDO and LDO-SB samples had a strong negative effect on their adsorption capacity to CR dye (but did not affect MB). Therefore, they (LDO and LDO-SB) were directly used for studying adsorption without the washing process as in the case of LDH and LDH-SH.

Some previous studies demonstrated that when Mg/Al-LDH was calcinated at temperature higher than 500 °C, the BET surface area of the calcinated Mg/Al-LDH (also known as Mg/Al-LDO) decreased. For example, Gennequin et al. [17] reported the S_{BET} value of the Mg/Al-LDH solid (77 m^2/g) and the Mg/Al-LDH samples calcined at 500, 600, 700, 800, and 900 °C (214, 188, 132, 122, and 111 m^2/g, respectively). In contrast, the S_{BET} value of carbon spheres remarkably increased from 13.8 to 464 m^2/g within increasing temperatures from 300 to 1,000 °C [21]. However, a higher temperature than 500 °C can thermally degrade some oxygen-containing functional groups on the surface of the carrier (i.e., carbon spheres). Those functionalities have a great contribution in keeping LDH or LDO in its surface (see Section 1-3. Surface Functionality). As a result, the structure of the synthesized composites might be not stable at high temperature; therefore, 500 °C was selected in this study.

3. Property of the Prepared Materials

The scanning electron microscopy (SEM) image and energy dispersive X-ray (EDS) data (detected by JSM-6510 LV) were used to observe the morphology and primary elements on the surface of the prepared materials. X-ray powder diffraction (XRD) (D6 Advance Bruker) was applied to detect their crystalline structure. The XRD data played an essential role in confirming the presence of the LDH or LDO minerals (or synthesized clays) on the resultant composites. The main functionality on their surface was recognized by Fourier-transform infrared spectroscopy (FTIR; IR Nicolet iS10). Before analyzing FTIR, the materials were pelleted with KBr. Textural properties of the materials were calculated from the adsorption/desorption isotherm of nitrogen at −196 °C (PMI's BET-Sorptometer). The electrical state of the material was analyzed by the common drift method, and the pH value at the point of zero charge was denoted as pH_{PZC}.

4. Adsorption Study

The removal process of Congo red (CR) or methylene blue (MB) dyes by the composites and their feedstocks was evaluated through batch experiments at a fixed solid/liquid (m/V) ratio of 0.5 g/L. In general, approximately 0.1 g of each dried adsorbent was transferred into a 300-mL Erlenmeyer flask. The flask contained 200 mL of single dye solution. The pH of dye solution had been adjusted before adding the adsorbent. The flask (solid-liquid mixture) was shaken at 150 rpm in a water bath shaker. The dye concentration was analyzed by ultraviolet-visible spectroscopy (UV-vis; Hitachi U2900). The solution of dyes was adjusted to pH 7.0 before analysis to avoid a mistake [22,23]. The the maximum absorption wavelength (λ_{max}) of CR and MB was 498 nm and 664 nm, respectively.

The amount of each dye adsorbed by the material at equilibrium (q_e; mg/g) and any time t (q_t; mg/g) was directly calculated from Eqs. (1) and (2), respectively:

$$q_e = \frac{(C_0 - C_e) \times V}{m} \quad (1)$$

$$q_t = \frac{(C_0 - C_t) \times V}{m} \quad (2)$$

where the parameters (C_0, C_e, and C_t) are the concentrations (mg/L) of the dye in solution (at the beginning, equilibrium, and any time t, respectively); m (g) is the dry mass of the material used; and V (L) is the volume of the dye solution.

A pH-dependent study was conducted at different initial pH solutions of dye (CR: ~800 mg/L or MB: 200 mg/L) from 2.0 to 10. The adsorption process was completed at 30 °C for 24 h. The residual dye concentration was detected after pH had been adjusted to neutral. The chemical stability of composites was evaluated under different pH values of distilled water, ranging from 2.0 to 10. After shaking at 30 °C for 24 h, the concentrations of Mg and Al leached from the composites were analyzed.

Adsorption kinetics was investigated at pH 7.0, 30 °C, and initial dye concentration of 210 mg/L for CR or 51 mg/L for MB. Adsorption isotherm was studied at different initial dye concentration (50–510 mg/L for MB and 50–1,000 mg/L for CR), pH 7.0, 24 h, and 30 °C. Adsorption thermodynamics was examined as the adsorption isotherm with the additional temperatures at 10 °C and 40 °C.

5. Adsorption Model

For adsorption kinetics, three common adsorption kinetic mod-

els were used to describe the time-dependent data of adsorption process. Those models (Eqs. (3), (4), and (5)) comprised the pseudo-first-order [24], pseudo-second-order [25], and Avrami model [26], respectively. They have been frequently applied in some previous studies [6,11,12,18], and their derivation has been summarized elsewhere [22,27].

$$q_t = q_e[1-\exp(-k_1 t)] \quad (3)$$

$$q_t = \frac{q_e^2 k_2 t}{1+q_e k_2 t} \quad (4)$$

$$q_t = q_e[1-\exp(-(k_{AV}t)^{n_{AV}})] \quad (5)$$

where q_t, q_e, and C_t are defined in Eq. (2); k_1 (1/min), k_2 [g/(mg·min)], and k_{AV} (1/min) are the rate constant of the pseudo-first-order, pseudo-second order, and Avrami models, respectively; and n_{AV} is the fractional adsorption order of the Avrami model.

For adsorption isotherm, three common models were applied to describe the adsorption behaviour. They included the Langmuir (Eq. (6)), Freundlich (Eq. (7)), and Redlich-Peterson (Eq. (8)). Those models have been commonly applied in the literature for the liquid-solid adsorption process [6,11,12,18]. More information on those models is available at the documents [22,27].

$$q_e = \frac{Q_{max} K_L C_e}{1+K_L C_e} \quad (6)$$

$$q_e = K_F C_e^{nF} \quad (7)$$

$$q_e = \frac{K_{RP} C_e}{1+a_{RP} C_e^g} \quad (8)$$

where Q_{max} (mg/g) is the maximum adsorption capacity of the material toward each dye; K_L (L/mg) is the Langmuir equilibrium constant; K_F [(mg/g)/(L/mg)^n] is the Freundlich constant, n_F (0<n<1) is the Freundlich intensity parameter; K_{RP} (L/g) and a_{RP} (L/mg)^g are the Redlich-Peterson constants; and g (0<g<1) is an exponent of the Redlich-Peterson model.

The thermodynamic parameters (ΔG^o, ΔH^o, and ΔS^o) of the adsorption process were estimated based on the equilibrium constant of the adsorption isotherm [18,27]. The Gibbs free energy change of the adsorption was directly calculated from Eq. (9).

$$\Delta G^o = -RT\ln K^o_{Equilibrium} \quad (9)$$

The relationship among the three thermodynamic parameters (ΔG^o, ΔH^o, and ΔS^o) is provided in Eq. (4):

$$\Delta G^o = \Delta H^o - T\Delta S^o \quad (10)$$

By substituting Eq. (9) into Eq. (10), the van't Hoff equation was achieved.

$$\ln K^o_{Equilibrium} = \frac{-\Delta H^o}{R} \times \frac{1}{T} + \frac{\Delta S^o}{R} \quad (11)$$

The non-linear form of the van't Hoff equation is expressed as follows:

$$K^o_{Equilibrium} = \exp\left(\frac{-\Delta G^o}{R}\right) \quad (12)$$

where $K^o_{Equilibrium}$ or KEq (L/mol) is obtained from the Langmuir constant (K_L; L/mol) by assumption the adsorption conducted under the standard state, and R is a gas constant [8.31 J/(mol·K)].

RESULTS AND DISCUSSION

1. Property of the Synthesized Composites

1-1. Surface Morphology

The surface morphology of the synthesized composites (Fig. 2)

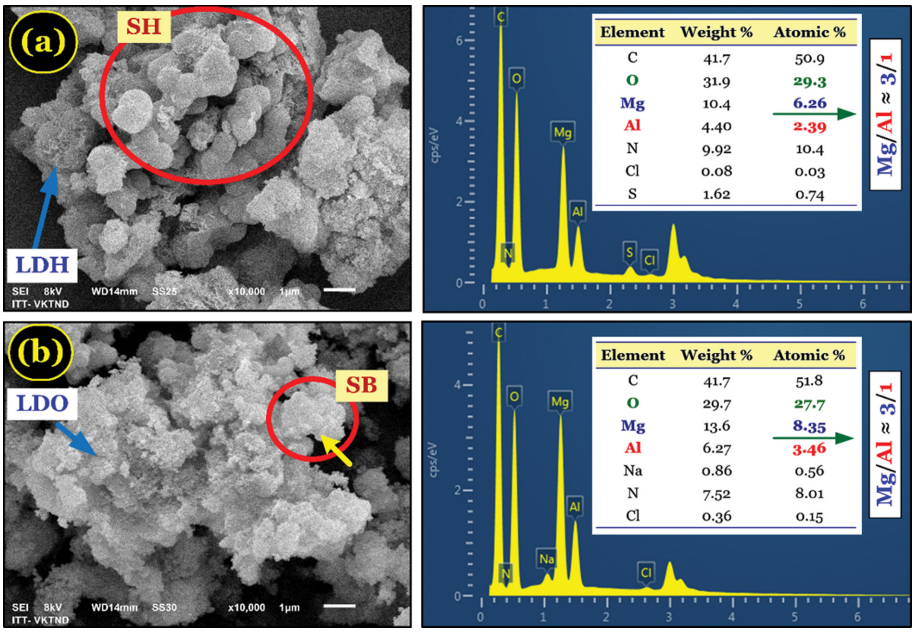

Fig. 2. SEM-EDS data of the prepared composites: (a) Layer double hydroxides-spherical hydrochar (LDH-SH) and (b) layer double oxides-spherical biochar (LDH-SB).

and their precursors (Fig. S2) is observed by the SEM technique. Fig. S2(a)-(b) shows that SH and SB had a spherical morphology, which is similar to the literature [18,19]. Meanwhile, LDH possessed a platelet-like layer morphology (Fig. S2(c)). This is a typical morphology of clay-like materials [10,16]. In contrast, LDO (Fig. S2(d)) was losing its original morphology and becoming a rock-like one [12,16,17].

Clearly, the synthesized composite (LDH-SH or LDO-SB) exhibited the morphological combination between LDH and SH or between LDO and SB (Fig. 2). Therefore, the SEM image visibly confirmed that LDH (or LDO) with its nanostructure and nanoparticle sizes was successfully retained on the surface of SH (or SB, respectively) (Fig. 2) through some functional groups. Those groups will be further discussed by the FTIR data.

1-2. Crystal Structure

The XRD profiles (Fig. S3) confirmed that the carbon materials (SH and SB) were amorphous [18], which is similar to activated carbon [28]. In contrast, the XRD spectrum of LDH (Fig. 3(a)) suggested that LDH exhibited a high crystallinity with its hydrotalcite-like phase (JCPDS No: 00-014-0191) and hexagonal-shaped crystallite [4,10,16].

The basal spacing of LDH related to the (003) plane (d_{003}) was calculated based on Bragg's law (Eq. (13)). The basal spacing of LDH and LDH-SH was calculated as 0.781 nm and 0.776 nm, respectively. Those values are similar to that of some other LDH materials, such as Zn/Al-LDH (0.777 nm) [14], Mg/Co/Al-LDH (0.775 nm) [9], Zn/Al-LDH (0.7630 nm) [16], and Mg/Al-LDH (0.7450 nm) [16]. Furthermore, the average crystallite size ($D_{average}$; Eq. (14)) of LDH was calculated based on the Scherrer equation (the validity for 5 nm<$D_{average}$<200 nm) and the reference [4]. The $D_{average}$ value of LDH (24±1.07 nm) was double that of LDH-SH (11.9±1.94 nm).

$$d_{(003)} = \frac{\lambda}{2\sin\theta} \tag{13}$$

$$D_{average} = \frac{K\lambda}{\beta\cos\theta} \tag{14}$$

where λ (0.154056 nm) is the typical wavelength of Cu Kα radiation; β (radian) that is the full width at half maximum of peak of the (006) and (110) planes was obtained from the Origin program; K (~0.89) is a shape factor; and θ (degree) is the relevant Bragg angle.

After calcining at 500 °C, layered double hydroxides (LDH) were converted to layered double hydroxides (LDO) [6,16]. This is because of the common dehydration of LDH by calcination that was supported by XRD (Fig. 3(b)) [6,14,16]. However, this conversion was not fully completed under 500 °C because a hydrotalcite-like structure (the 2θ peak at around 11.3° and 34.4°) was still detected in the LDO and LDO-SB samples [17].

Under such calcination temperature, a crystalline periclase MgO was performed (Fig. 3(b)) [17]; therefore, the $d_{(003)}$ and $D_{average}$ values of LDO were not available for calculation. For example, the $D_{average}$ value of LDO (3.98 nm) and LDO-SB (3.03 nm) estimated by the Scherrer equation was out of the valid range (5-200 nm). As expected, the composite LDH-SH or LDO-SB (Fig. 3) exhibited the crystal phase in the XRD spectrum similar to its precursor (LDH or LDO). To some extent, the composites can be classified as semi-crystalline because their structure comprised of crystalline and amorphous regions.

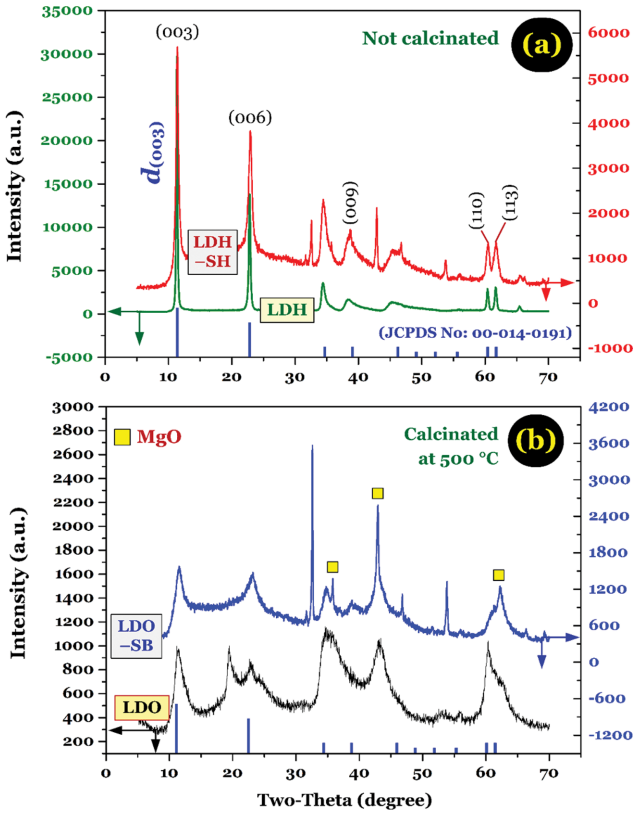

Fig. 3. XRD data of the composites and their clay-like feedstocks under conditions (a) not calcinated (LDH and LDH-SH) and (b) calcinated at 500 °C (LDO and LDO-SB).

1-3. Surface Functionality

The main surface functionality of six prepared materials was analyzed by the FTIR technique (Fig. 4). LDH and LDO were inorganic material, whereas the opposite was true for SH and SB (carbonaceous material). Therefore, they exhibited different surface functionalities. For example, LDH contained the host anions (i.e., CO_3^{2-}) in its interlayer region and positively charged hydroxide groups on its external surface (Fig. 4(a)). The presence of CO_3^{2-} anions and OH groups can be identified at the band of around 1,370 cm^{-1} (C=O) and 3,430 cm^{-1} (O-H), respectively [6,12,16,17].

In contrast, SH and SB (Fig. 4(b)) contained mainly oxygen functional groups (~3,430, 1,700, and 1,208 cm^{-1} corresponding to OH, C=O, and C-O) and aromatic rings in its carbonaceous structure (~1,604 and 1,020 cm^{-1} relative to C=C and C-H, respectively) [18-20].

Notably, when LDH or LDO was assembled on the surface of SH or SB (Fig. 2), some functional groups on the surface of SH or SB could act as strong adsorbing sites to retain the LDH or LDO nanoparticles. Several functional groups in the inorganic and carbonaceous materials were not detected in the composites LDH-SH and LDO-SB, suggesting that they were consumed during the hydrothermal carbonation process to generate the composites.

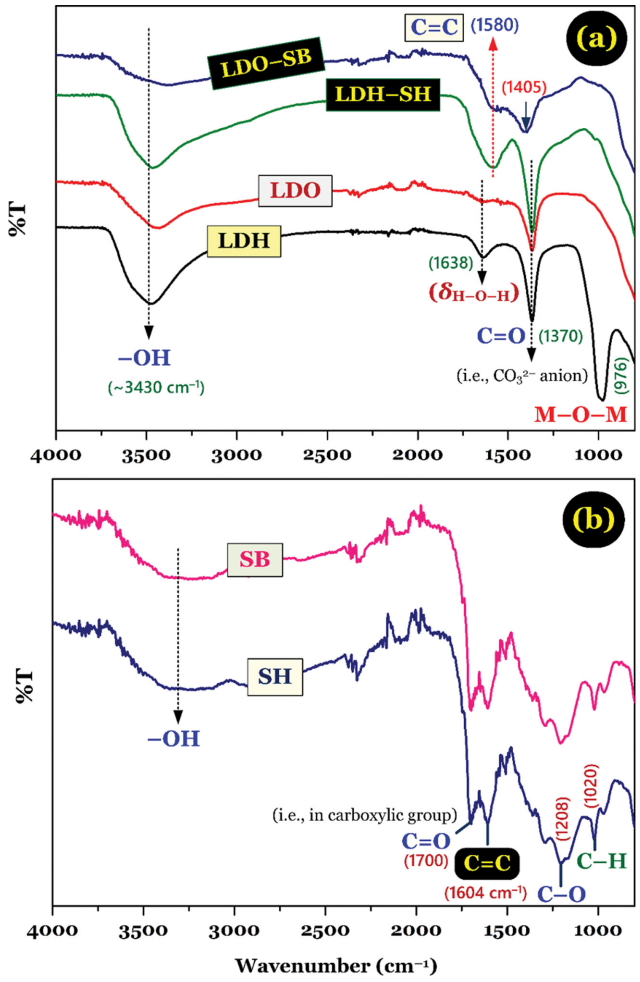

Fig. 4. FTIR spectrum of the composites (LDH-SH and LDO-SB) and their feedstock (SH, SB, LDO, and LDH).

They included the C=O in carboxylic groups, C-O in lactonic groups, and aromatic C-H groups (Fig. 4). These have been identified as active groups for adsorbing cationic and anions dye through hydrogen bonding, n-π interaction, and π-π interaction [5,29,30]. The consumption of these groups (derived from the carbonaceous materials) can lead to decreasing the adsorption capacity of the composites.

1-4. Textural Features

The textural properties of SH, SB, LDH, LDO, LDH-SH, and LDO-SB that were obtained from nitrogen adsorption/desorption isotherm at 77 K are provided in Table 1. The result demonstrated that spherical hydrochar and spherical biochar were non-porous and microporous materials (their S_{BET} of 7.08 and 220 m^2/g, respectively), which agrees with the literature [18,20].

In contrast, layered double hydroxides and oxides are categorized as a mesoporous material, with their S_{BET} (m^2/g) and average pore width (nm) being 40.4 and 79.7 m^2/g and 46.0 and 29.1 nm, respectively. Lei et al. [6] also reported the S_{BET} and average pore width of Ni/Mg/Al-LDHs (101 m^2/g and 23.4 nm) and Ni/Mg/Al-LDOs (179 m^2/g and 15.7 nm). A similar observation was reported by Gao and coworkers [16] for calcinated Mg/Al-LDH (also known as Mg/Al-LDO; 71.2 m^2/g and 22.2 nm). Furthermore, after calcining at 500 °C, the surface area of the material was improved, for example, the S_{BET} of LDO (79.7 m^2/g; Table 1) being remarkably higher than that of LDH (40.4 m^2/g). Similarly, Gennequin et al. [17] found that the S_{BET} value of Mg/Al-LDO (ranging from 112 to 224 m^2/g dependent on the calcination temperatures) was remarkably higher than that of Mg/Al-LDH (77 m^2/g). They explained that the increase in the S_{BET} value was due to LDO exhibiting a higher crystallization than LDH [17].

Meanwhile, the composites LDH-SH and LDO-SB mainly exhibited the mesoporous nature of LDH and LDO. In general, six prepared materials (7.08-220 m^2/g; Table 1) had lower S_{BET} value compared to activated carbon (AC), such as commercial AC (1,026 m^2/g) [30], prepared non-spherical AC (812-1,413 m^2/g) [29], and prepared spherical AC (1,125-1,191 m^2/g) [20]. Therefore, the role of pore filling in the adsorption mechanism of the dyes (MB and CR) was less important than other mechanisms, such as hydrogen bonding.

1-5. Chemical Stability

The chemical stability of the composite was evaluated though the effect of pH on the amount of Mg and Al ions leached from the composites. The composites were generated from the inorganic LDH and LDO and organic SH and SB feedstocks. Unlike the organic materials, the inorganic ones were synthesized from the coprecipitation process at a high pH value of 12. Thus, under strong acid conditions (pH<3.0), their current structure was not stable. This conclusion was confirmed by the leaching test in Fig. 5(a)-(b).

2. Adsorption Property of the Synthesized Composites

2-1. Effect of Solution pH

As previously discussed in Fig. 5, the composites exhibited poor chemical stability under pH 2.0. In addition, under strong basic conditions (pH>10), the chemical structure of CR and MB dyes

Table 1. Textural properties of the composites and their feedstocks

	Unit	Before adsorption						After CR adsorption	
		SH	SB	LDH	LDO	LDH-SH	LDO-SB	LDH-SH	LDO-SB
S_{BET}	m^2/g	7.08	220	40.4	79.7	58.5	198	54.8	18.1
S_{Ext}	m^2/g	—	50	32.0	59.9	48.9	127	46.8	10.5
S_{Micro}	m^2/g	—	170	8.35	19.8	9.61	70.9	7.93	7.58
V_{Total}	cm^3/g	0.008	0.114	0.464	0.580	0.319	0.440	0.301	0.204
L_o	nm	—	2.07	46.0	29.1	21.8	8.89	21.9	45.1

Note: BET surface area (S_{BET}), external surface area (S_{Ext}), micropore surface area (S_{Micro}), average pore width (L_o).

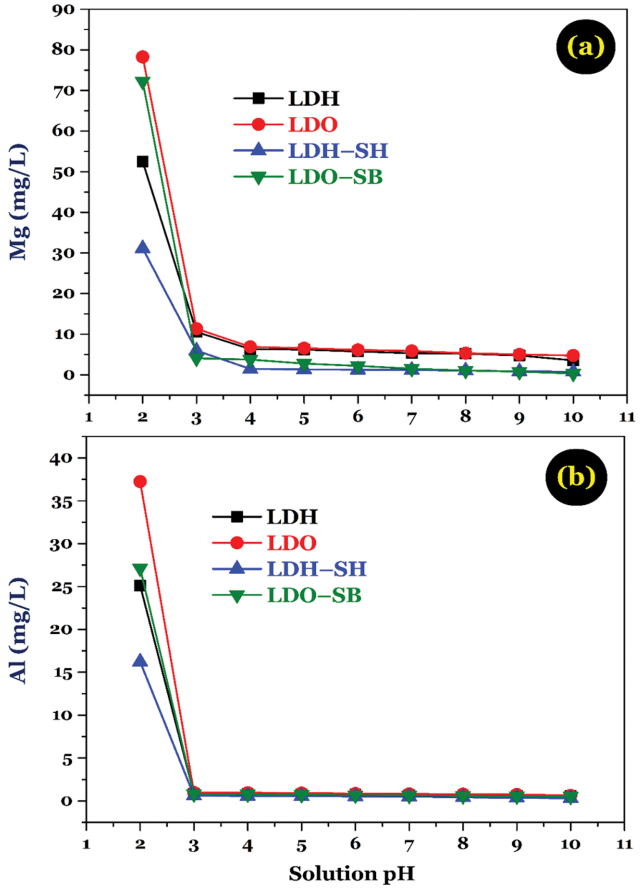

Fig. 5. Chemical stability of the composites under different solution pH values.

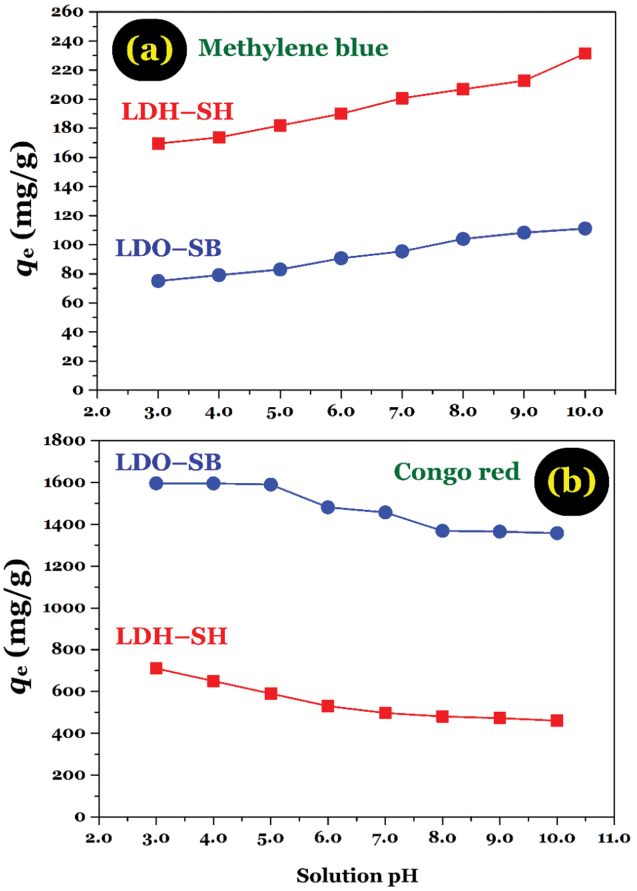

Fig. 6. Effect of pH on the adsorption process of (a) MB and (b) CR dye by the composites.

was changed [23]. Therefore, a pH-dependent study of adsorption was conducted from pH 3.0 to 10 (Fig. 6(a)-(b)).

The change of the surface charge of the materials under different solution pH was detected by their pH_{PZC} (Fig. S4). A material usually possesses a predominantly negatively charged surface when solution pH is higher than its pH_{PZC}. Carbon spheres (i.e., SH and SB) often contain a high content of oxygen-functional groups that are mainly acidic groups with their low p*K*a values as carboxylic groups (p*K*a~3.0-4.0) [19]. Therefore, their pH_{PZC} is often lower than 7.0, such as 4.62 (for SH) and 5.55 (for SB). In contrast, clay-like materials (i.e., LDH and LDO) often exhibit a positively charged surface [2,4] because of the abundant OH groups (p*K*a~9.0-10) on their surface [13]. Thus, the pH_{PZC} values of LDH (8.47) and LDO (10.5) were remarkably higher than the carbon spheres. Notably, the composites LDH-SH and LDO-SB exhibited a charge nature on their surface similar to their inorganic LDH and LDO than organic SH and SB feedstocks, with their pH_{PZC} being 6.98 for LDH-SH and 10.1 for LDO-SB.

Fig. 6(a)-(b) shows the different trends for adsorbing anionic CR and cationic MB dyes by two composites. The adsorption capacity of two composites toward MB cations (Fig. 6(a)) increased within an increase in solution pH from 3.0 to 10, whereas the opposite was true for adsorbing CR anions (Fig. 6(b)). A similar phenomenon was observed by other researchers [31] for adsorbing CR and MB dyes by the synthesized alumina-zirconia composite. Notably, the LDH-SH composite was more favorable to adsorb MB; while LDO-SB well adsorbed CR. Those phenomena were presumably because of the different primary adsorption mechanisms among them. The adsorption mechanisms will be thoroughly discussed in Section 3. Feasible Adsorption Mechanisms.

2-2. Adsorption Kinetics

The time-dependent data of adsorption are represented in Fig. 7. In general, the adsorption process took rapidly place during the first contact period of 30 min. This means that more than 50% dye was removed from solution within a 30-min adsorption. Notably, the adsorption process of CR dye by LDO-SB reached equilibrium after 30 min of contact, whereas the opposite was true for the adsorption of MB dye (~300 min). The result suggests that the LDO-SB composite had a higher affinity for adsorbing CR anions than MB cations.

Table 2 shows the parameters of the adsorption kinetics of dyes by the prepared materials. According to higher adj-R^2 (the adjust coefficient of determination) and lower red-χ^2 (the reduced chi-square statistic) values, it can be concluded that the experimental data of time-dependent adsorption were better described by the Avrami model (0.978-0.999 for adj-R^2 and 0.023-238 for red-χ^2) than the pseudo-second-order model (0.813-0.993 and 0.521-1,719) and the pseudo-first-order model (0.273-0.943 and 0.914-4,543,

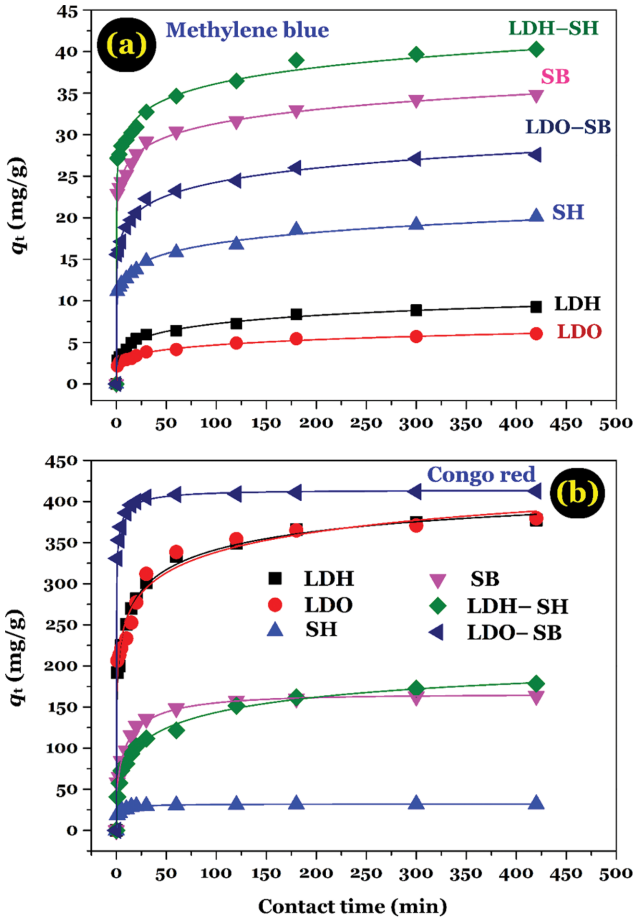

Fig. 7. Effect of contact time on the adsorption processes of (a) methylene bule and (b) Congo red dyes by the composites and their feedstocks.

respectively).

The adsorption rate constant (k_A) was determined by the Avrami model. The k_A values (1/min) for the adsorption process of CR dye by the prepared materials decreased as the following order: LDO-SB (6.315/min)>SH (0.6010/min)>SB (0.0981/min)>LDH-SH (0.0141/min)>LDH (0.0647/min)>LDO (0.0178). The result suggests that using the LDO-SB composite remarkably increased the removal rate of CR dye from water compared to their feedstocks.

2-3. Adsorption Isotherms

Fig. 8 provides the adsorption isotherms of two MB and CR dyes by two composites (LDH-SH and LDO-SB) at different solution temperatures (10, 30, and 40 °C). The isotherm for adsorbing CR dye by both composites (Fig. 8(c) and (d)) was categorized as H-shape [30,32]. Meanwhile, for the adsorption of MB dye, the isotherm was H-shape for LDH-SH and L-shape for LDO-SB. The result suggests that LDH-SH and LDO-SB exhibited a high affinity to adsorbing anionic CR dye, especially under low concentration of dye feedstock. A similar conclusion was obtained for adsorbing cationic MB dye by LDH-SH.

In this study, some common isotherm models that include the Langmuir, Freundlich, and Redlich-Peterson models were applied for modelling the adsorption process. Among them, the Redlich-Peterson model described the experimental data of the equilibrium adsorption better than did the Langmuir and Freundlich models. This is because this model indicates a lower red-χ^2 and higher adj-R^2 values than the others (Table 3).

The Langmuir maximum adsorption capacity (Q_{max}) of the composites at 30 °C followed the order of anionic Congo red dye: 1,589 mg/g (LDO-SB)>499 mg/g (LDH-SH) and cationic methylene blue dye: 226 mg/g (LDH-SH)>78.6 mg/g (LDO-SB). The result suggests that the two developed composites exhibited an excellent ad-

Table 2. Parameters of the adsorption kinetics of methylene blue and Congo red dyes by the composites and their feedstocks

	Methylene blue dye						Congo red dye					
	LDH	LDO	SH	SB	LDH-SH	LDO-SB	LDH	LDO	SH	SB	LDH-SH	LDO-SB
1. Pseudo-first-order model												
q_e	7.84	4.98	15.0	28.6	33.1	21.6	293	294	28.0	123	112	391
k_1	7.7E-02	9.6E-02	6.1E+06	7.1E+09	1.4E+02	1.8E+12	132	133	36738	57.8	59.5	150
adj-R^2	0.791	0.672	0.636	0.777	0.780	0.659	0.579	0.583	0.754	0.409	0.273	0.943
red-χ^2	1.50	0.91	9.44	17.7	23.2	17.7	4543	4480	19.2	1497	2104	709
2. Pseudo-second-order model												
q_e	8.39	5.26	16.7	30.7	35.2	24.2	345	341	31.0	161	166	406
k_2	1.4E-02	3.2E-02	5.4E-02	5.3E-02	5.3E-02	3.4E-02	1.4E-03	1.6E-03	3.4E-02	1.4E-03	6.3E-04	8.8E-03
adj-R^2	0.886	0.813	0.817	0.894	0.877	0.871	0.887	0.840	0.974	0.957	0.923	0.993
red-χ^2	0.821	0.521	4.75	8.42	12.9	6.72	1217	1719	2.01	109	222	91.6
3. Avrami model												
q_e	14.7	54.8	112	97.1	154	55.8	432	502	32	165	212	414
k_A	2.5E-03	3.2E-08	2.3E-09	4.0E-07	2.7E-09	1.5E-04	6.5E-02	1.8E-02	6.0E-01	9.8E-02	1.4E-02	6.3E+00
n_A	0.275	0.191	0.118	0.093	0.087	0.134	0.239	0.196	0.345	0.454	0.355	0.241
adj-R^2	0.992	0.992	0.991	0.996	0.992	0.995	0.994	0.978	0.995	0.991	0.996	0.999
red-χ^2	0.054	0.023	0.231	0.337	0.827	0.238	68.3	238	0.420	22.7	10.9	10.0

Note: The units of q_e (mg/g), k_1 (1/mim), k_2 [g/(mg·min)], and k_A (1/min).

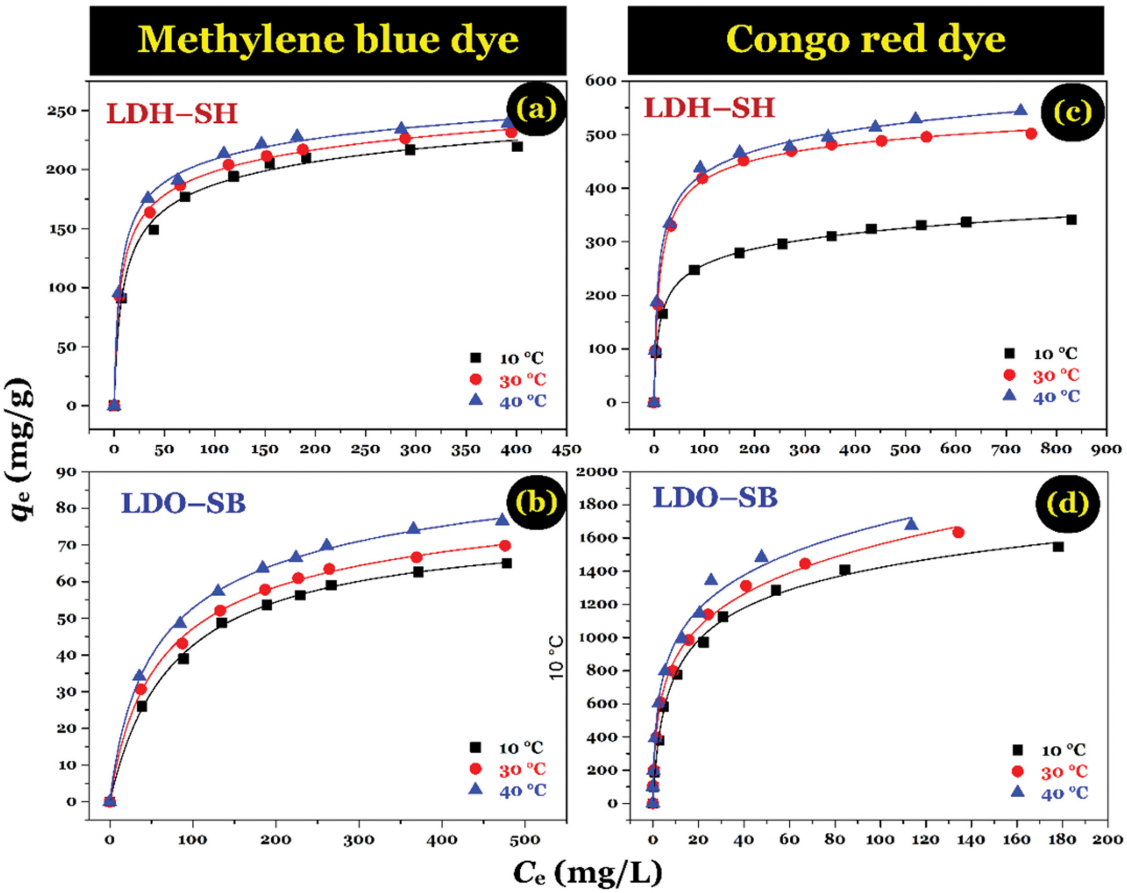

Fig. 8. Adsorption isotherm of (a) methylene blue and (b) Congo red dyes onto the composites and their feedstocks (the non-linear fitting of the Langmuir model).

Table 3. Parameters of target adsorption isotherms of Congo red and methylene blue dyes by the prepared composites (LDH-SH and LDO-SB) at different solution temperatures (10, 30, and 40 °C)

	Congo red dye						Methylene blue dye					
	LDH-SH			LDO-SB			LDH-SH			LDO–SB		
	10 °C	30 °C	40 °C	10 °C	30 °C	40 °C	10 °C	30 °C	40 °C	10 °C	30 °C	40 °C
1. Langmuir model												
Q_{max}	330	499	517	1550	1589	1626	221	226	234	75.7	78.6	85.6
K_L	0.059	0.069	0.082	0.101	0.136	0.179	0.073	0.101	0.116	0.013	0.015	0.017
adj-R^2	0.978	0.992	0.981	0.985	0.967	0.962	0.983	0.984	0.985	0.999	0.998	0.997
red-χ^2	290	261	688	4598	10612	12783	90.6	96.9	98.0	0.509	1.26	1.65
2. Freundlich model												
K_F	93.9	144	150	354	414	478	73.5	82.5	89.5	9.46	11.8	13.6
n	0.201	0.202	0.205	0.304	0.294	0.281	0.194	0.182	0.175	0.322	0.296	0.288
adj-R^2	0.979	0.947	0.961	0.960	0.981	0.977	0.978	0.981	0.976	0.980	0.987	0.989
red-χ^2	275	1710	1435	12083	6109	7634	119	115	153	8.76	6.60	6.73
3. Redlich-Peterson model												
K_{PR}	39.9	48.6	77.7	277	856	991	29.3	42.1	46.4	0.9984	1.4917	1.9009
a_{RP}	0.246	0.143	0.267	0.353	1.427	1.440	0.229	0.314	0.314	0.014	0.034	0.040
g	0.886	0.937	0.904	0.860	0.788	0.803	0.902	0.904	0.915	0.989	0.923	0.905
adj-R^2	0.999	0.997	0.998	0.996	0.997	0.989	0.995	0.999	0.998	0.999	0.998	0.999
red-χ^2	9.88	90.6	71.7	1227	1075	3883	28.2	5.47	11.8	0.586	0.821	0.559

Note: the unit of Q_{max} (mg/g), K_L (L/mg), K_F (mg/g)/(mg/L)^n, K_{PR} (L/g), a_{RP} (L/mg)^g, and the others (no unit)

Table 4. Thermodynamic parameters of adsorption of methylene blue and Congo red by the composites and their feedstocks

	T (K)	Adsorption of MB					Adsorption of CR				
		Van't Hoff equation	K_{Eq}	ΔG^o	ΔH^o	ΔS^o	Van't Hoff equation	K_{Eq}	ΔG^o	ΔH^o	ΔS^o
LDH-SH	283	y=−1369x+14.9	23,442	−23.68	11.38	124	y=−934x+13.3	18,798	−23.2	7.76	109
	303	R^2=0.999	32,442	−26.17	(11.3)	(124)	R^2=0.933	21,916	−25.2	(8.13)	(110)
	313		37,205	−27.39	(adj-R^2=0.999)			26,269	−26.5	(adj-R^2=0.858)	
LDO-SB	283	y=−1070x+11.7	2,706	−18.6	8.90	97.1	y=−1631x+16.3	32,266	−24.4	13.6	134
	303	R^2=0.991	3,381	−20.5	(9.07)	(97.7)	R^2=0.965	43,605	−26.9	(11.8)	(128)
	313		3,918	−21.5	(adj-R^2=0.978)			57,352	−28.5	(adj-R^2=0.864)	

Note: The units of ΔG^o (kJ/mol), ΔH^o (kJ/mol), and ΔS^o [J/(mol·K)]; the values in parentheses (for the ΔH^o and the ΔS^o) obtaining from the non-linear form of the van't Hoff equation.

sorption capacity to the anionic dye than cationic dye. Clearly, LDO-SB (1,589 mg/g) well adsorbed CR molecules better than LDH-SH (499 mg/g). However, LDH-SH (226 mg/g) was more favorable to adsorbing MB molecules than LDO-SB (78.6 mg/g). This might be due to the difference in existing adsorption mechanisms among them (Section 3. Feasible Adsorption Mechanisms).

In general, LDO-SB (Q_{max}=1,589 mg/g) exhibited an outstanding adsorption capacity to Congo red dye compared to many materials in the literature. They include NMA-LDHs calcined at 600 °C (or Ni/Mg/Al layered double oxides; Q_{max}=1,250 mg/g) [6], carbon nanotube/Mg(Al)O nanocomposites (1,250 mg/g) [5], flower-like porous microspheres derived from Ni/Al-LDHs (1,229 mg/g) [7], magnetic polydopamine Mg/Al-LDH nano-flakes (585 mg/g) [8], chitosan hydrogel beads impregnated with carbon nanotubes (450 mg/g) [33], and commercial activated carbon (491 mg/g) [34], polyacrylamide-modified hydroxo aluminum/graphene composites (424 mg/g) [35], rice straw biochar (191 mg/g) [36], wood chip biochar (110 mg/g) [36], Mg/Fe-LDHs (105 mg/g) [37], Korean cabbage biochar (96 mg/g) [36], and Mg/Al-LDHs (37 mg/g) [10].

2-4. Adsorption Thermodynamics

Effect of solution temperatures on the adsorption process was evaluated through the adsorption isotherm (Fig. 8), and the Langmuir maximum adsorption capacity of the composites at different temperatures is listed in Table 3. The adsorption capacity of two composites toward two target dyes increased when solution temperatures increased from 10 °C to 40 °C (Table 3). This is consistent with the sign of the changes in enthalpy (ΔH^o) in Table 4.

The thermodynamic parameters of the adsorption process (ΔG^o, ΔH^o, and ΔS^o) are provided in Table 4. A negative value of ΔG^o suggests that the adsorption process occurred spontaneously without any supported energy. Positive ΔH^o value indicates that the adsorption process was endothermic. Similarly, Lei et al. [6] reported that the adsorption process of CR dye by Ni/Mg/Al LDOs was endothermic. The change in entropy (ΔS^o) of the adsorption process was positive (97.1-134 J/mol·K), suggesting that the dye molecular (CR or MB) organized at the interface (composite/solution) becomes random during the adsorption. Notably, the adsorption process had a low magnitude of ΔH^o (7.76-13.6 kJ/mol), suggesting relatively weak adsorption (mainly physical adsorption) [38].

3. Feasible Adsorption Mechanisms

Two composites exhibited different properties; therefore, the primary adsorption mechanisms might be dissimilar. The adsorption mechanisms in this study were discussed at pH 7.0 and 30 °C. Under this pH value, the surface chare of LDH-SH (its pH_{PZC} of 6.98) and LDO-SB (10.1) was nearly neutral and predominantly positive, respectively.

3-1. For Dye Adsorption Mechanism by LDH-SH

The LDH-SH composite was prepared from a soft carbonaceous material (spherical hydrochar; SH) and layered double hydroxides (LDH). Although π-π interaction has been identified as the primary adsorption mechanism of aromatic dyes onto carbonaceous materials such as biochar [18] and activated carbon [30], such mechanism is less important for hydrochar [39]. Therefore, the π-π interaction plays a less important role in the adsorption mechanism of two target dyes.

Similarly, pore filing had a minor contribution to the adsorption mechanism because LDH-SH had a low BET surface area. Table 1 shows the S_{BET} value of CR-laden LDH-SH (54.8 m^2/g) was similar to that of pristine LDH-SH (58.5 m^2/g), confirming again this conclusion.

LDH-SH exhibited a positively changed surface (mainly from $-OH_2^+$ group in the external surface of LDH), electrostatic attraction was highly expected for adsorbing CR anions [9]. However, LDH-SH still well adsorbed MB cations, which resulted from the

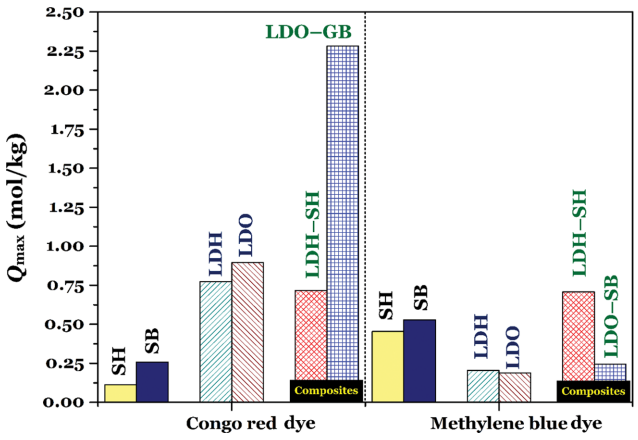

Fig. 9. Comparison of the Langmuir maximum adsorption capacity (Q_{max}) of the composites (LDH-SH and LDO-SB) and their feedstocks: carbonaceous material (spherical hydrochar and spherical biochar) and clay-like materials (layered double hydroxides and layered double oxides).

great contribution of SH (Fig. 9). Two kinds of hydrogen bonding interactions might also play an integral role in adsorbing MB dyes. A dipole-dipole H-bonding interaction can occur between H-donor (from the composite) and H-acceptor (from the dye molecular) [40]. In this case, the hydrogen atoms on the surface of the composite (i.e., in the hydroxyl or carboxylic groups) act as H-donor; meanwhile, the atoms (i.e., nitrogen and oxygen) of the dye act as H-acceptor. Another interaction is commonly known as Yoshida H-bonding. This interaction can mainly occur between the aromatic rings in dye molecules and the hydroxyl groups on the composite's surface [18,19,36].

3-2. For Dye Adsorption Mechanism by LDO-SB

The LDO-SB composite was generated from LDH-SH through a further carbonization at 500 °C. Under such carbonization, the LDH feedstock was dehydrated to LDO (see XRD data); meanwhile, the hydrochar (SH) feedstock was converted to biochar (SB), which is known as a hard carbonaceous material. In essence, π-π interaction has been reported as a primary adsorption mechanism of dye onto commercial AC [30], glucose-based AC [19,20], and biochar [18,36]. Although π-π interaction played an important role in adsorption two dyes onto LDO-SB compared to LDH-SH, it was not the primary adsorption mechanism. In fact, if such interaction is dominant, the feedstock (biochar, SB) will exhibit excellent adsorption capacity for two dyes (Fig. 9). A similar conclusion was obtained for hydrogen bonding interactions.

Notably, LDO-SB had a higher adsorption capacity to anionic CR dye than cationic MB dye because it has a positively charged surface (i.e., mainly $-OH_2^+$ from LDO). Therefore, the electrostatic attraction was one of the most dominant mechanisms for absorbing CR anions in solution. An identical conclusion was reported by other authors [9] for adsorbing methyl orange dye by the composite of LDO and graphene.

Unlike LDH-SH, pore filling played an important role for absorbing the dye by LDO-SB. Table 1 shows that the S_{BET} value of LDO-SB remarkably decreased from 198 to 18.1 m^2/g after CR adsorption. The result suggests the important role of pore filling in the adsorption mechanism.

During the adsorption of anionic dyes, the LDO in the LDO-SB composite was restructured. This means that CR dye can act as active guest anions to simulate the structural regeneration of LDO into LDH through the unique property of LDH-based material ("memory effect") [2,9,17]. A similar phenomenon (the regeneration mechanism of LDO in the presence of guest organic anions) has been reported by Gao and coworkers [16] for the adsorption of different natural humic acids (HA) onto Mg/Al-LDO and Zn/Al-LDO.

LDO-SB (Q_{max}=2.281 mol/kg; Fig. 9) exhibited an overwhelmingly higher adsorption capacity than its feedstock (1.153 mol/kg; 0.895 mol/kg for LDO and 0.258 mol/kg for SB). The result suggests that LDO-SB exhibited an excellent adsorption capacity to CR dye resulting from the great contribution of LDO. In other words, the LDO feedstock had a significantly higher contribution to adsorbing CR dye in solution than SB. If assuming new contributions (adsorption mechanisms) is not performed, the remarkable higher adsorption capacity of CR dye by the LDO-SB composites compared to LDO might be due to higher adsorption sites. In fact, the alone LDO nano-particles often tend to cluster together (aggregation phenomenon) compared to that in the LDO-SB composites. This phenomenon has been observed by Gao and colleagues [16] for Mg/Al-LDO and Zn/Al-LDO. The LDO-SB composite was prepared from the LDO and SB feedstocks through hydrothermal carbonization. This synthesis process can decrease the aggregation of LDO nano-particles on the surface of the resultant LDO-SB composite. Because the adsorption was conducted in the same experimental condition (especially the same dried mass of adsorbents; Eq. (1)), LDO-SB exhibited higher adsorption sites (as well as adsorption capacity) than its LDO feedstock.

CONCLUSIONS

The composites LDH-SH and LDO-SB were successfully developed from the clay-like materials, LDH and LDO, and the carbon spheres, SH and SB, through simple hydrothermal carbonization. The composites exhibited the combination properties of their different kinds of the feedstock. Through hydrothermal carbonization, LDH nanocrystals were successfully assembled to the surface of hydrochar (SH) to generate LDH-SH. A further carbonization at 500 °C did not affect the stability of the composite LDO-SB. LDH-SH was favorable to adsorb cationic MB dye, while LDO-SB was excellent adsorbent for adsorbing anionic CR dye. The maximum adsorption capacity of LDO-SB to CR was 1,589 mg/g, and that of LDH-SH to MB was 226 mg/g at 30 °C.

ACKNOWLEDGEMENT

This research is funded by Vietnam National Foundation for Science and Technology Development (NAFOSTED) under grant number 103.02-2019.54.

SUPPORTING INFORMATION

Additional information as noted in the text. This information is available via the Internet at http://www.springer.com/chemistry/journal/11814.

REFERENCES

1. I. Ihsanullah, *Chem. Eng. J.*, **388**, 124340 (2020).
2. H. N. Tran, D. T. Nguyen, G. T. Le, F. Tomul, E. C. Lima, S. H. Woo, A. K. Sarmah, H. Q. Nguyen, P. T. Nguyen, D. D. Nguyen, T. V. Nguyen, S. Vigneswaran, D.-V. N. Vo and H.-P. Chao, *J. Hazard. Mater.*, **373**, 258 (2019).
3. F. Z. Janani, N. Taoufik, H. Khiar, W. Boumya, A. Elhalil, M. Sadiq, A. V. Puga and N. Barka, *Sur. Interfaces*, **25**, 101263 (2021).
4. T. L. P. Galvão, C. S. Neves, A. P. F. Caetano, F. Maia, D. Mata, E. Malheiro, M. J. Ferreira, A. C. Bastos, A. N. Salak, J. R. B. Gomes, J. Tedim and M. G. S. Ferreira, *J. Colloid Interface Sci.*, **468**, 86 (2016).
5. S. Yang, L. Wang, X. Zhang, W. Yang and G. Song, *Chem. Eng. J.*, **275**, 315 (2015).
6. C. Lei, X. Zhu, B. Zhu, C. Jiang, Y. Le and J. Yu, *J. Hazard. Mater.*, **321**, 801 (2017).
7. W. Huang, X. Yu and D. Li, *RSC Adv.*, **5**, 84937 (2015).

8. J. Li, Q. Fan, Y. Wu, X. Wang, C. Chen, Z. Tang and X. Wang, *J. Mater. Chem. A*, **4**, 1737 (2016).
9. T. S. Kazeem, M. Zubair, M. Daud, N. D. Mu'azu and M. A. Al-Harthi, *Korean J. Chem. Eng.*, **36**, 1057 (2019).
10. R.-r. Shan, L.-g. Yan, Y.-m. Yang, K. Yang, S.-j. Yu, H.-q. Yu, B.-c. Zhu and B. Du, *J. Ind. Eng. Chem.*, **21**, 561 (2015).
11. Y. Wang, T. Du, L. Zhou, Y. Song, S. Che and X. Fang, *Korean J. Chem. Eng.*, **35**, 709 (2018).
12. F. Yang, S. Zhang, Y. Sun, D. C. W. Tsang, K. Cheng and Y. S. Ok, *J. Hazard. Mater.*, **365**, 665 (2019).
13. H. N. Tran, C.-C. Lin, S. H. Woo and H.-P. Chao, *Appl. Clay Sci.*, **154**, 17 (2018).
14. P. Kowalik, M. Konkol, M. Kondracka, W. Próchniak, R. Bicki and P. Wiercioch, *Appl. Catal. A-Gen.*, **464-465**, 339 (2013).
15. G. E. d. S. dos Santos, P. V. d. S. Lins, L. M. T. d. M. Oliveira, E. O. d. Silva, I. Anastopoulos, A. Erto, D. A. Giannakoudakis, A. R. F. d. Almeida, J. L. d. S. Duarte and L. Meili, *J. Clean. Prod.*, **284**, 124755 (2021).
16. Z. Gao, K. Sasaki and X. Qiu, *Langmuir*, **34**, 5386 (2018).
17. C. Gennequin, T. Barakat, H. L. Tidahy, R. Cousin, J. F. Lamonier, A. Aboukaïs and S. Siffert, *Catal. Today*, **157**, 191 (2010).
18. H. N. Tran, F. Tomul, H. T. H. Nguyen, D. T. Nguyen, E. C. Lima, G. T. Le, C.-T. Chang, V. Masindi and S. H. Woo, *J. Hazard. Mater.*, **394**, 122255 (2020).
19. F.-C. Huang, C.-K. Lee, Y.-L. Han, W.-C. Chao and H.-P. Chao, *J. Taiwan Inst. Chem. Eng.*, **45**, 2805 (2014).
20. H. N. Tran, Y.-C. Wen, Y.-F. Wang and S.-J. You, *Environ. Technol.*, **40**, 1376 (2019).
21. H. N. Tran, C.-K. Lee, T. V. Nguyen and H.-P. Chao, *Environ. Technol.*, **39**, 2747 (2018).
22. H. N. Tran, S.-J. You, A. Hosseini-Bandegharaei and H.-P. Chao, *Water Res.*, **120**, 88 (2017).
23. Q. Zhou, C. Xie, W. Gong, N. Xu and W. Zhou, *J. Hazard. Mater.*, **198**, 381 (2011).
24. S. K. Lagergren, *Sven. Vetenskapsakad. Handingarl*, **24**, 1 (1898).
25. G. Blanchard, M. Maunaye and G. Martin, *Water Res.*, **18**, 1501 (1984).
26. A. Putnis, *Kinetics of mineral processes*, An Introduction to Mineral Sciences, Cambridge University Press, Cambridge (1992).
27. É. C. Lima, M. H. Dehghani, A. Guleria, F. Sher, R. R. Karri, G. L. Dotto and H. N. Tran, *CHAPTER 3 - Adsorption: Fundamental aspects and applications of adsorption for effluent treatment*, Green Technologies for the Defluoridation of Water, Elsevier (2021).
28. B. Koo and S. P. Jung, *Chem. Eng. J.*, **424**, 130388 (2021).
29. H. N. Tran, S.-J. You and H.-P. Chao, *J. Environ. Manage.*, **188**, 322 (2017).
30. H. N. Tran, Y.-F. Wang, S.-J. You and H.-P. Chao, *Process Saf. Environ. Prot.*, **107**, 168 (2017).
31. A. O. Adesina, O. A. Elvis, N. D. S. Mohallem and S. J. Olusegun, *Environ. Technol.*, **42**, 1061 (2021).
32. C. Moreno-Castilla, *Carbon*, **42**, 83 (2004).
33. S. Chatterjee, M. W. Lee and S. H. Woo, *Bioresour. Technol.*, **101**, 1800 (2010).
34. N. Kannan and M. Meenakshisundaram, *Water Air Soil Pollut.*, **138**, 289 (2002).
35. Y. Wu, H. Luo and H. Wang, *Sep. Sci. Technol.*, **49**, 2700 (2014).
36. D. D. Sewu, P. Boakye and S. H. Woo, *Bioresour. Technol.*, **224**, 206 (2017).
37. I. M. Ahmed and M. S. Gasser, *Appl. Surf. Sci.*, **259**, 650 (2012).
38. R. Chang and J. W. Thoman, Jr., *Phys. Chem. Chemi. Sci.*, 779 (2014).
39. H. N. Tran, S.-J. You and H.-P. Chao, *Korean J. Chem. Eng.*, **34**, 1708 (2017).
40. M. Paredes-Laverde, M. Salamanca, J. D. Diaz-Corrales, E. Flórez, J. Silva-Agredo and R. A. Torres-Palma, *J. Environ. Chem. Eng.*, **9**, 105685 (2021).

Supporting Information

Composites derived from synthetic clay and carbon sphere: Preparation, characterization, and application for dye decontamination

Nguyen Duy Dat*, Ton That Loc,***, Mai Thuan Trieu*, Dong Thanh Nguyen****, Khuong Quoc Nguyen*****, My Linh Nguyen*, Anh Duy Duong Le******,*******, and Hai Nguyen Tran**,***,†**

*Faculty of Chemical & Food Technology, Ho Chi Minh City University of Technology and Education, Thu Duc, Ho Chi Minh, 700000, Vietnam
**Institute of Fundamental and Applied Sciences, Duy Tan University, Ho Chi Minh, 700000, Vietnam
***Faculty of Environmental and Chemical Engineering, Duy Tan University, Da Nang, 550000, Vietnam
****Institute of Environmental Technology, Vietnam Academy of Science and Technology, Hanoi, Vietnam
*****Department of Crop Science, College of Agriculture, Can Tho University, Can Tho, Vietnam
******Computational Optics Research Group, Advanced Institute of Materials Science, Ton Duc Thang University, Ho Chi Minh City, Vietnam
*******Faculty of Applied Sciences, Ton Duc Thang University, Ho Chi Minh City, Vietnam
(*Received 4 July 2021 • Revised 20 August 2021 • Accepted 24 August 2021*)

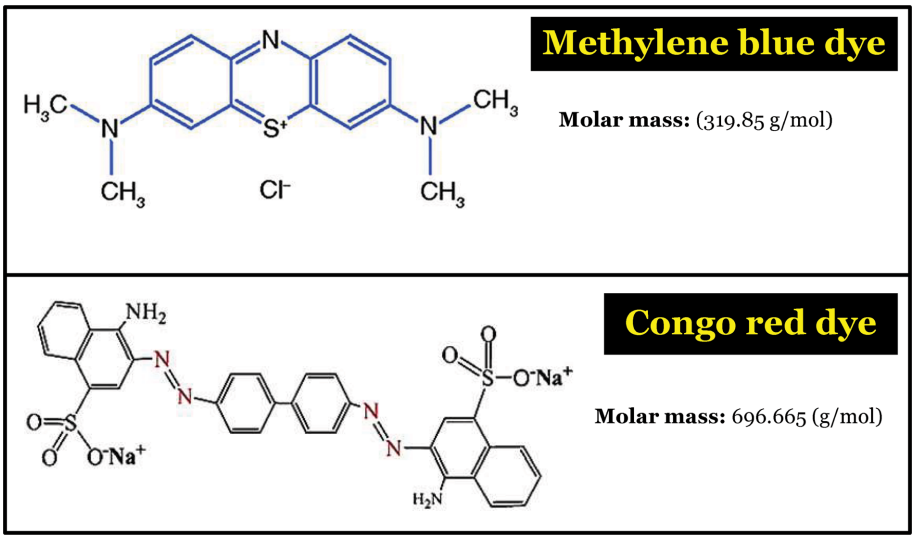

Fig. S1. Chemical structure of methylene blue (MB) dye and Congo red (CR) dye.

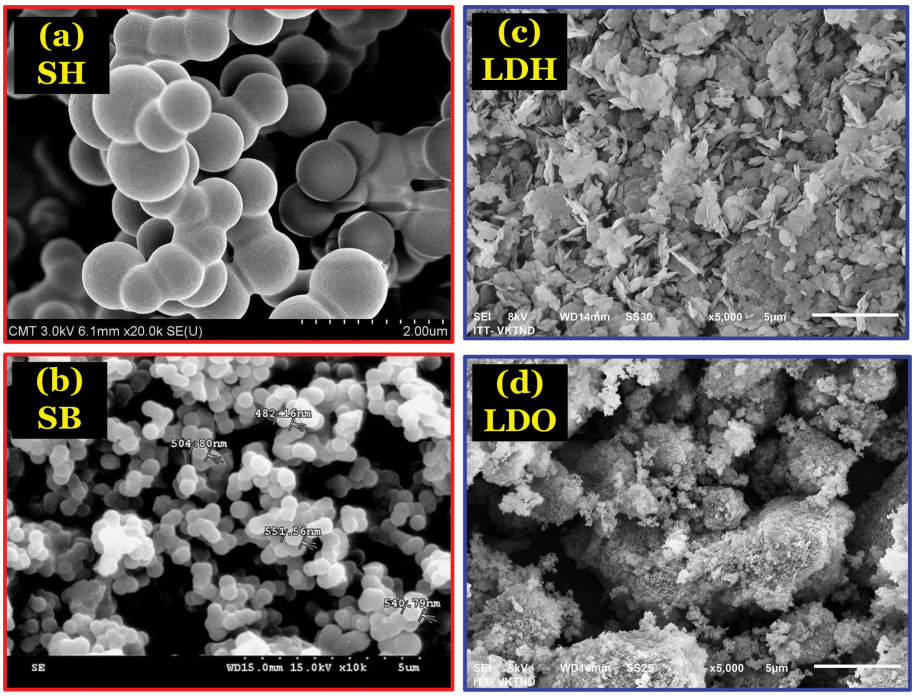

Fig. S2. SEM images of (a) glucose hydrochar, (b) glucose biochar, (c) layered double hydroxides, and (d) layered double oxides.

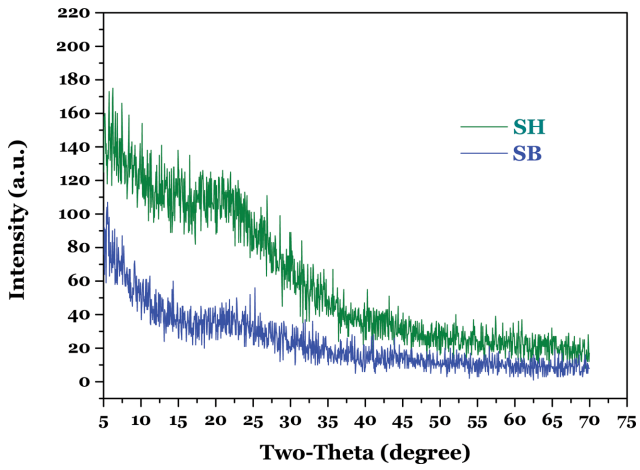

Fig. S3. XRD data of glucose hydrochar (SH) and biochar (SB).

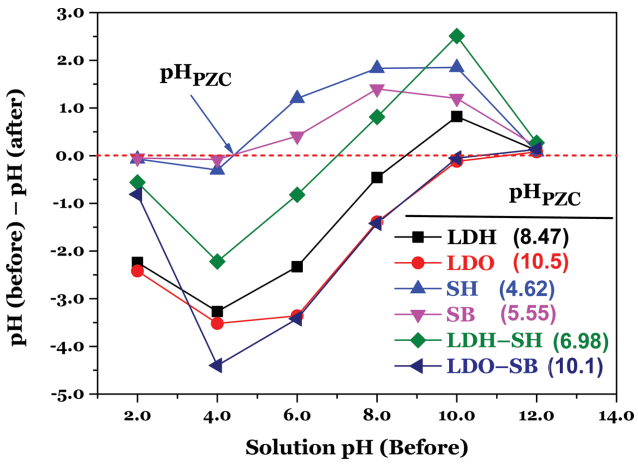

Fig. S4. pH_{PZC} of the prepared materials.